HAL
open science

Self-organized patterns by a DC pin liquid anode discharge in ambient air: Effect of liquid types on formation

Shiqiang Zhang, Thierry Dufour

To cite this version:

Shiqiang Zhang, Thierry Dufour. Self-organized patterns by a DC pin liquid anode discharge in ambient air: Effect of liquid types on formation. Physics of Plasmas, 2018, 25 (7), pp.073502. 10.1063/1.5030099 . hal-02377964

HAL Id: hal-02377964

https://hal.science/hal-02377964

Submitted on 24 Nov 2019

HAL is a multi-disciplinary open access archive for the deposit and dissemination of scientific research documents, whether they are published or not. The documents may come from teaching and research institutions in France or abroad, or from public or private research centers.

L'archive ouverte pluridisciplinaire **HAL**, est destinée au dépôt et à la diffusion de documents scientifiques de niveau recherche, publiés ou non, émanant des établissements d'enseignement et de recherche français ou étrangers, des laboratoires publics ou privés.

This document is a pre-print version. You may use it at your own convenience although its content may deviate in places from the final published article.

Title	**Self-organized patterns by a DC pin liquid anode discharge in ambient air: Effect of liquid types on formation**
Authors	Shiqiang Zhang, and Thierry Dufour
Affiliations	LPP, CNRS, UPMC Univ. Paris 06, Ecole Polytech., Univ. Paris-Sud, Observatoire de Paris, Université Paris-Saclay, Sorbonne Universités, PSL Research University, 4 Place Jussieu, 75252 Paris, France. E-mail: thierry.dufour@sorbonne-universite.fr
Ref.	Physics of Plasmas 25, 073502 (2018)
DOI	https://doi.org/10.1063/1.5030099
Abstract	A pin liquid anode DC discharge is generated in open air without any additional gas feeding to form self-organized patterns (SOPs) on various liquid interfaces. Axially resolved emission spectra of the whole discharge reveal that the self-organized patterns are formed below a dark region and are visible mainly due to the N_2 ($C^3\Pi$-$B^3\Pi$) transitions. The high energy N_2 (C) level is mainly excited by the impact of electrons heated by the local increased electric field at the interface. For the first time, the effect of the liquid type on the SOP formation is presented. With almost the same other discharge conditions, the formed SOPs are significantly different from HCl and H_2SO_4 liquid anodes. The SOP difference is repeated when the discharge current and gap distance change for both liquid anodes. The variations of SOP size and discretization as a function of discharge current and gap distance are discussed and confirm that different SOPs are formed by the HCl liquid anode from tap water or the H_2SO_4 liquid anode. A possible explanation is brought up to explain the dependence of SOPs on the liquid type.

I. Introduction

To date, plasma liquid interactions (deionized water, tap water, saline, or electrolyte solution) draw increasing attention due to their great potential applications in plasma medicine,[1,2] plasma agriculture,[3,4] nanomaterials synthesis,[5,6] and water purification.[7] In plasma activated media (PAM), longlived reactive species such as H_2O_2, HNO_2, HNO_3 and $ONOO^-$ are generated or diffused into liquid from the plasma. As an example, the production of H_2O_2 in an aqueous medium can result from a gas discharge plasma interaction as found in Ref. 8. HNO_2 is another paramount species verified to diffuse from the plasma to the liquid via the interface region.[9] As a result, it is of utmost importance to investigate the physical and/or chemical processes at the interface that determines the aqueous amounts of species in liquid.[2]

Type of power supply	SOPs formed on a …	
	Plasma-solid interface	Plasma-liquid interface
AC	• Enclosed DBD[13-16] • APPJ impinging on ITO in open air[17]	• Pin liquid electrode discharge in open air[18, 19]
DC	• CBLD in noble gas on the cathode[20-24] • DBD with a semiconductor electrode[25] • Glow discharge at at 1 atm on the anode[26,27] and low pressure[28-32]	• Pin liquid electrode discharge in the air with auxiliary gas[33-35] and without[36-38].

Table 1. Types of plasma devices with formed self-organized patterns.

Plasma self-organized patterns (SOPs) among physical phenomena are likely to appear on a liquid or a solid interface, considering AC or DC power supplies as shown in Table I. It should be noted that besides the SOP formed at the plasma-liquid (or even solid) interface, patterns can be formed in the plasma as seen from the lateral side of the discharge chords.[10–12]

In parallel to experimental works, SOPs have been the subject of several theoretical studies considering various discharge configurations such as dielectric barrier discharge (DBD) discharge,[39,40] arc discharge,[41,42] and DC glow discharge.[43,44] Benilov modeled SOPs in DC glow discharge and/or arc discharge based on the first-principles equations containing all the relevant physical mechanisms and proposed that the cathode sheath instability is responsible for SOP formation on the cathode.[43] Bieniek et al. also applied the same approach to simulate SOPs formed on the anode of DC glow discharge and found that the anode SOPs are related to the change in the sign of the near anode voltage.[44] Trelles obtained SOP results, which is in quite good agreement with experimental observations but for arc discharge.[45] Raizer and Mokrov owed SOP formation to the instabilities caused by thermal expansion and/or electric field redistribution.[15] Gopalakrishnan et al. studied solvated electrons but not SOPs in a pin liquid discharge in argon by a particle-in-cell/Monte Carlo model.[46] To date, no simulation work reports SOP formation in pin liquid discharge in air to the best of the authors' knowledge.

Obviously, the SOPs on the cold solid anode of DC discharges are the closest relative of SOP on cold liquid anodes of DC discharges that are studied in this work. However, there are still differences between them. Replacing a metal electrode with a liquid electrode in the vicinity of the air discharge increases its water content,[47] which changes the stability of the discharge48 and hence SOP formation experimentally. Additionally, due to larger specific heat capacity of water than the metals (generally one order of

magnitude larger), the gas temperature decreases, making the discharge not easy to turn in strong filamentary or even arc discharge.[49] The auxiliary gas, such as helium,34 could also lower the gas temperature and establish the comparatively stable discharge and reproducible SOP formation.

Comparing the work of Refs. [36] and [37] to that of Ref. 34, for a pin liquid electrode discharge configuration, the use of auxiliary gas is not necessary to form the luminous SOPs in open air. Moreover, electric conductivity (EC) is experimentally verified to determine the SOP formation with a NaCl solution electrode in Ref. 34 and a water electrode in Ref. 37. However, the effect of the liquid type on SOP formation is never reported yet. Considering the luminescence, although the spectra of SOP under different discharge setups are observed, there is no underlying mechanism for the analysis of the observed spectra either for the moment.

In this work, the dependence of SOPs on liquid types (different chemical compositions of anode liquid) is reported for the first time. Using the specific pin liquid anode discharge, the line-of-sight integrated emission spectra with axial resolution are presented, and the underlying mechanism of the SOP spectra is analyzed. Moreover, the behavior of the self-organized patterns with discharge current and the gap distance under different liquid anodes (tap water, HCl solution, and H_2SO_4) confirms the dependence of the SOPs on the liquid type. Finally, an attempting explanation is brought on the liquid type influence on SOP formation.

II. Experimental setup

The discharge setup is shown in Fig. 1. A DC power supply (FuG, type HCN 350M-6500, 0–6.5 kV, 0–30 mA) is connected to a high power ballast resistor (Sfernice, RSS 30 265, 111 kΩ) to stabilize the atmospheric pressure plasma. An aluminum pin is employed as a cathode above the liquid anode with varying gap distances. The pin has a diameter of 3.2mm and is sharpened at the end. Stainless steel submerged in the liquid (electrolyte solution), which is filled in a quartz vessel (height, 13 mm; diameter, 57 mm), is connected to the anode of the power supply. A spectrometer (Andor Shamrock SR 303i-A) is used to determine the line-of-sight integrated plasma emission from the lateral side of the discharge chord. The electrical conductivity (EC) is quantified using a conductivity meter (HANNA HI-87314).

The chemical products used in this work are H2SO4 acid (500 ml, for the determination of nitrogen, >97.5%, CAS No.: 7664-93-9; Sigma Aldrich/Merck), HCl acid (1 L; MIEUXA), and HF acid (for analysis, EMSUR, 48%; Sigma Aldrich/Merck).

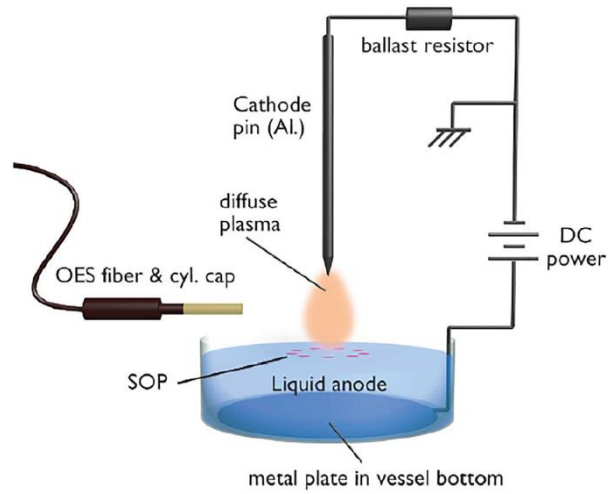

Fig. 1. Schematics of the pin liquid anode DC discharge setup.

III. Results & Discussions

III. A. Axially resolved optical emission

III.A.1. OES spectra results

A typical DC pin liquid anode discharge is pictured in Fig. 2(a). It is clearly observed that a pear-shaped and homogeneous discharge is emitted by the cathode pin and a self-organized pattern (SOP) of plasma lying on the liquid anode interface. Also, a dark region separates these two emissive plasma regions, with a typical thickness of 1mm at the center and 2mm in periphery. Finally, the apparent color of the diffuse plasma is rather yellowish, while it is purplish for the SOP. In order to perform a finer analysis, the discharge is characterized by optical emission spectroscopy. The optical fiber (capped with the 1mm inner diameter capillary) is placed at 6 different vertical positions between the anode and the cathode, while the interelectrode distance remains fixed at 6mm upon the entire experiment. The discharge emission is estimated between 200 and 700 nm every mm along the vertical axis and reported in the 200–500 nm range in Fig. 2(b). The main bands identified are the N_2 second positive system (SPS, $C^3\Pi$-$B^3\Pi$), the OH ($A^2\Sigma^+$-$X^2\Pi$) transition, and the NO ($A^2\Sigma^+$-$X^2\Pi$) system. Figure 3 reports the axial profile of these bands along gap distances and the total plasma emission in the 200–700nm range. It is worth mentioning that no hydrogen (656 nm), oxygen (777 nm, 844 nm), or even nitrogen atomic lines (>700 nm) could be detected in any optical fiber position with this aluminum pin electrode.

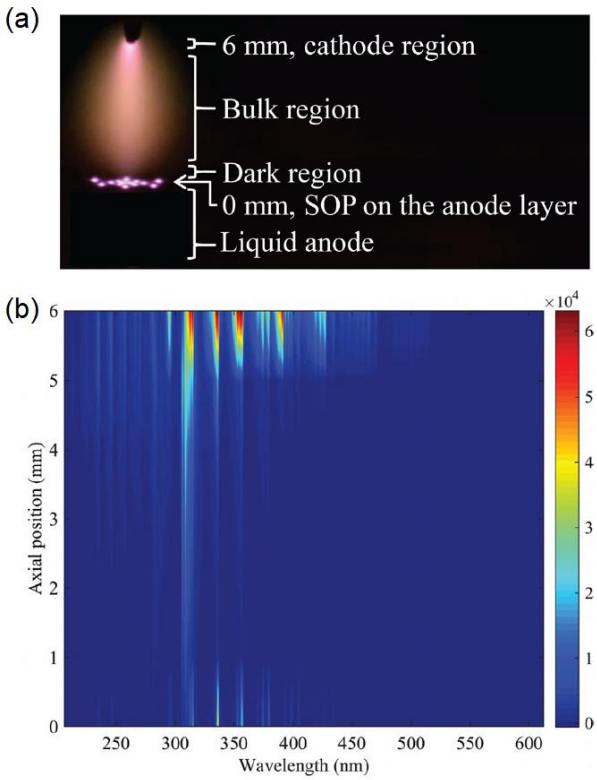

Fig. 2. (a) Picture of the pin liquid anode discharge taken using a camera and (b) the axially resolved optical emission spectrum of the discharge. The exposure time for (b) is 50 ms, and the employed grating is 600 grooves/mm. The discharge voltage is 1150 V, the current 18.5 mA, and EC=2.66 mS/cm. The emission spectra are acquired from axial 0mm to 6mm with a 1mm step.

III.A.2. Analysis of pin liquid discharge and SOP emissions

Combining camera pictures and optical emission spectroscopy (OES) spectra allows us to state that the discharge is stratified into 4 main regions: (i) between 5 and 6 mm, a cathode region which is highly emissive with several molecular nitrogen and nitric oxide bands, as well as the OH band headed at 310 nm; (ii) between 5 and 1 mm, a bulk region characterized by an overall decay of the discharge emission, in particular the N_2 SPS bands whose emissions are wallowed in the background. The OH band emission decreases as one moves closer to the liquid anode but much slower, so that it is still significant at 1mm compared with N_2 SPS bands; (iii) between roughly 1 and 0.5mm appears the dark region: its thickness is much thinner along the main vertical axis than on the lateral edges of the discharge. This region is correlated not only with the minimum emission of $N_2(C^3\Pi\text{-}B^3\Pi)$ and NO ($A^2\Sigma^+\text{-}X^2\Pi$) transitions, as shown in Fig. 2(b), but also with the total plasma emission, which is the lowest at 1mm (Fig. 3); (iv) finally, between 0.5mm and 0 mm, the anode region (or layer) is characterized by an unexpected significant rise of $N_2(C^3\Pi\text{-}B^3\Pi)$, while OH ($A^2\Sigma^+\text{-}X^2\Pi$) and NO($A^2\Sigma^+\text{-}X^2\Pi$) are negligible (1 order of magnitude smaller). SOPs are generated in this anode region and seem to mostly result from physicochemical pathways, inducing the excitation of molecular nitrogen. The fact that N_2 ($C^3\Pi\text{-}B^3\Pi$) dominates the emission of SOPs on the liquid interface is consistent with other different types of discharge setups, such as a similar type in Refs. 36 and 50, a plasma jet colliding with the water surface,[51] surface discharge over water in Ref. 52, water falling film DBD in Ref. 53, or in other types of pin liquid discharge systems.[19,34,54]

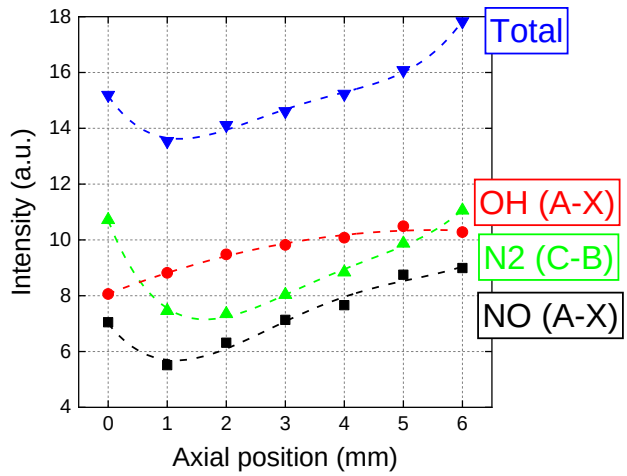

Fig. 3. Axial distribution of OH(A-X) (309 nm), NO(A-X)(236.3 nm), $N_2(C^3\Pi\text{-}B^3\Pi)$ (337.1 nm), and total emission with the intensity on a logarithmic scale.

Note that in a similar DC pin liquid anode discharge operating also in open air,[50] the spatial stratification is different. Indeed, the authors obtained a comparatively thicker luminous anode region and no evident dark region above the luminous anode region. In addition, they have Faraday dark space and a cathode space which do not appear in this work. The disparity might be due to the material of the pin electrode, where an aluminum pin is used here rather than stainless steel in their work. As a matter of fact, the authors also tried to change the polarity of the discharge, to apply a copper pin or a carbon pin, or change liquid to a metal plate as above. However, when the polarity changed, there are no such SOP patterns formed with the aluminum (Al) pin anode and liquid cathode, only to find a strong discharge column. When the copper or carbon pin cathode is used, the formed SOP on the liquid anode is not stable enough even to perform the measurements. The used configuration is the most stable type we tried. For the structure of the pin cathode and liquid anode, the authors presume that the pin material and fine shape of the pin tip greatly affect stability and SOP formation.

The plausible chemical pathways producing OH and NO radicals and excited N_2 molecules are listed in Table II.

	Reactions	Typical rate constants	References
R_1	$e^- + H_2O \rightarrow OH(A/X) + H + e^-$	10^{-18}–10^{-16} $m^3 s^{-1}$ [a]	55 and 56
R_2	$e^- + OH(X) \rightarrow OH(A) + e^-$	10^{-14}–10^{-13} $m^3 s^{-1}$ [a]	56 and 57
R_3	$e^- + H_3O^+ \rightarrow OH + H_2$	10^{-13} $m^3 s^{-1}$	58
R_4	$e^- + O_2 + M \rightarrow O_2^- + M[O_2, N_2]$	10^{-43}–10^{-42} $m^6 s^{-1}$	59
R_5	$e^- + N_2(X) \rightarrow N_2(C) + e^-$	10^{-19}–10^{-16} $m^3 s^{-1}$ [a]	56 and 60
R_6	$N_2(A) + N_2(A) \rightarrow N_2(C) + N_2(X)$	10^{-16} $m^3 s^{-1}$	61
R_7	$N_2(A) + H_2O \rightarrow N_2 + H + OH$	$\leq 10^{-20}$ $m^3 s^{-1}$	62

Table II. Main chemical reactions in overall discharge and SOP region. Rate constants for electron impact dissociation and excitations are calculated from the cross-section in the given references with electron temperature T_e=1-3 eV.

a. Overall. In an air discharge, OH generation by thermal dissociation of water molecules could be negligible, as the rate coefficient is somewhat 4 orders lower than that of the electron dissociation (R_1 and R_3 in Table II). This is verified even for the gas temperature around 2000 K.[63]

b. Cathode region (5–6 mm). In the cathode region, the electrons are heated in the thin cathode fall layer (for the aluminum cathode in air, V_n≈300V, p≈3 µm, and E≈10^8 V/m). Here, high energetic electrons can dissociate water vapor from the surrounding atmosphere to produce most of the OH radical (R_1, ≈5 eV). This pathway may not occur further in the bulk region where the electron temperature is estimated to be less than 2 eV.[64] Another source of OH radical is from electron dissociative recombination (R_3), as hydrated H_3O^+ readily pops out in such a pin liquid anode device.[65] Note that the generation of OH by N_2(A) dissociation with H_2O (R_7) in ambient air is only comparable with the generation via R_1 or R_2 if the N_2(A) density is larger than 10^{19} m^{-3}.[66]

c. Bulk region (1–5 mm). As shown in Fig. 2(b), this region is solely dominated by the emission of OH ($A^2\Sigma^+$-$X^2\Pi$). This transition results from (i) the diffusion of the OH radicals produced in the cathode region and (ii) the excitation of the ground state OH to OH(A) by the electron impact (R_2).[48] As it approaches the liquid anode (T_{aq}≈330K), it is not surprising that the gas temperature decreases and the electric field intensity maintains a comparatively low level in the bulk region (the average electric field is 1.5×10^5 V/m considering the cathode fall). The reduced gas temperature and the electron temperature would enhance the three-body electron attachment to oxygen (R_4, the rate could be 10^{-17} $m^3.s^{-1}$, provided the air number density of 10^{25} m^{-3}). A decrease in the number of free electrons reduced the possibility of excitation of the ground OH radical, which makes the plasma emission from OH(A) decreases when it is further away from the pin electrode. This also leads to a decrease in the emission intensity of reactive nitrogen species [N_2(C) or NO(A)] when it approaches from the pin electrode to the anode.

d. Dark region (0.5–1mm). The formation of the dark region around the 1mm axial position correlates with a larger extent with the minimum emission of N_2 ($C^3\Pi$-$B^3\Pi$), as shown in Fig. 3. At atmospheric pressure, N_2 (C) is mainly excited by the direct electron impact of the ground state N_2 (X) (R_5), such as in a RF atmospheric pressure plasma jet (APPJ) effluent in open air with Te≈1.5 eV,[67] as opposed to the pooling reaction (R_6).[56,68] So, the decrease in free electrons also leads to reduced emission of N_2 ($C^3\Pi$-B3Π). The minimum emission of the dark region is found to be consistent with the results of an AC plate liquid electrode discharge in open air.[69]

e. Anode region (luminous anode layer, 0.5–0 mm). The anode region is marked by a sudden significant increase in the optical emission and the parallel formation of SOP [Figs. 2(b) and 3]. At the interface, the N_2 ($C^3\Pi$-$B^3\Pi$) emission mainly leads to the visible self-organized patterns [Fig. 2(b) at 0 mm]. Figure 3 shows that the intensity of N_2 SPS transition is significantly larger than the emission of the plasma bulk zone [mainly from OH(A)], hence, explaining why the so-called dark region is formed.

If one compares direct impact reactions to produce N_2(C) via R_5 or OH(A) via R_2, it turns out that the electron energy is somewhat two times larger to produce N_2(C) [≈11 eV (Ref. 70)] than to produce OH(A) [≈4 eV (Ref. 71)]. Therefore, more energetic electrons arise in the anode region, hence enabling the excitation of N_2(C) at the interface. At collision-frequent atmospheric pressure, the ohmic heating is the dominant heating mechanism of electrons,[72] which means that energetic electrons are heated by a local increased electric field. Nevertheless, no investigation of the electric field at the interface under such discharge is reported yet to verify the local increased electric field, although in Ref. 46 the model work on a DC pin liquid anode discharge in argon atmospheric pressure presented that at the interface, the electric field increased from ≈1.5×10^5 V/m to ≈6.5×10^5 V/m on the plasma side on a 0.1mm scale. Further measurement on the electric field is required.

Even if the spectrum of SOPs is characterized using OES, the mechanism for the regularity of SOP is not clear. The regularity of SOPs might also be the type of diffraction pattern of ionization waves40 launched from the pin. As ionization waves impinge at the liquid surface, the electric field at the SOPs is enhanced due to the interference of ionization waves and electrons are heated, which excites N_2(C) to the N_2(B) state as described above. However, this hypothesis needs further validation. In Sec. III B and III C, SOP behavior is studied by varying the discharge current and gap distance to better understand the SOP formation mechanism and to benchmark the SOP liquid type dependence.

III. B. Effects of the discharge current on SOP

III.B.1. Voltage-current characteristics and SOP appearance

The V–I characteristic of the DC discharge is shown in Fig. 4(a) where the discharge current is decreased from 37mA to 6mA by reducing the applied voltage. Decreasing the current induces a rise in the voltage up to a critical value of 1230V at 26mA. Then, a sudden voltage drop (or jump) is observed at 26mA immediately followed by a second voltage increase with a maximum as high as 1420V at 6mA. The sudden voltage drop at 26mA delimits the two regions shown in Fig. 4(a). In parallel to the V–I characteristic, pictures of the SOPs have been taken for different discharge currents, as shown in Fig. 4(b).

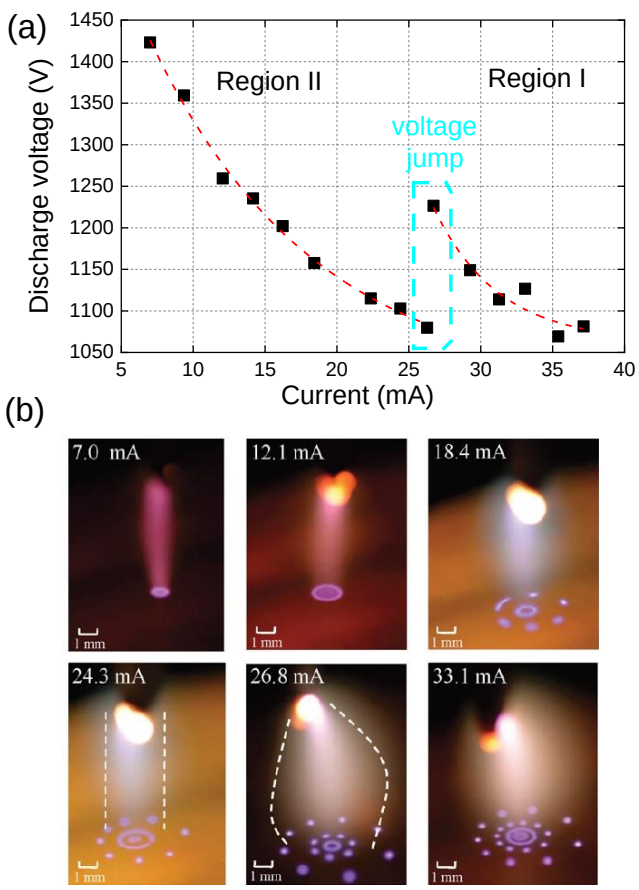

Fig. 4. (a) V-I characteristic of the DC discharge and (b) the pictures of the corresponding SOP obtained for several discharge currents. The gap distance between the pin and the liquid is 5 mm. Tap water is employed, and the electric conductivity is 2.36 mS/cm. The exposure time of the picture in (b) is 8 ms. The white dashed lines depict the discharge shape in two regions.

III.B.2. Discussions on SOPs evolution with discharge current

These SOPs can be described according to the parameters used in the studies reported in Table I, i.e., their size, their structural complexity (e.g., concentric rings,[19,34,36,37] strips,[34,37] spots,[19,34,37] or round area[19,34,35,37]), and their dynamics, e.g., rotations.[19,34,36] In region I (I>26 mA), the bulk discharge appears diffusive in a pear-shape[48,69] with an enlarged diameter close to the one of the SOPs formed on the liquid interface. This SOP shows a high complexity degree for larger currents. For example, at 33.4 mA, the pattern is structured onto 4 virtual concentrated circles: On the two outer circles, the plasma is discreet since it appears as spots distributed at equal distances from one another, while on the two inner circles, the plasma spots seem to recover, hence forming two uniform and distinct rings. Decreasing the current from 33.4mA to 26.8mA induces a loss in SOP complexity with a single outer discreet ring and two inner uniform rings. This uniform aspect could be correlated with the exposure time of the camera, which is as high as 8 ms. The dynamics of the inner circles could not only be faster than those of the outer circles but also scale on times much faster than 8ms. For this reason, one could consider this uniformity as solely apparent.

Transition from region I to region II is marked by a morphological change in the bulk plasma, which is now columnar close to the filamentary mode due to the larger electric field (E/N). The columnar discharge can be seen clearly in Figs. 4(b) at 12.1mA and 7.0mA. At discharge currents 18.4 and 24.3mA, the discharge is close to the filamentary discharge. In this region II, however, SOPs are still present with a lower pattern diameter and lower structural complexity. For currents at 18.4 and 24.3mA, SOPs show distinct and concentric rings although much lower in number and complexity. For currents lower than 12mA, the SOP is no more designed as concentric rings but as a unique and uniform spot whose diameter is close to the one of the bulk discharges, namely, 1.2mm.

SOPs at the interface evolve continuously, while the discharge current increases without presenting two distinct regions. Therefore, the discharge morphology change seems not directly correlated with SOP size and discretization. The decrease in the SOP diameter seems correlated with the decrease in the discharge current and therefore with a decrease in the electron density in the bulk discharge as discussed in Sec. IIIC. From the point of ionization waves, if larger discharge currents lead to stronger ionization waves, more outer spots of the SOP would have a stronger electric field, enabling there a higher heating of electrons and enhancing the emission of these outer spots. However, this relationship between discharge current and ionization waves still needs further validation.

III. C. Effect of the gap distance on SOP

III.C.1. Discharge characteristics and SOP appearance

As shown in Fig. 5(a), increasing the gap distance from 1 to 11mm induces a linear decrease in the discharge current and a rise in the plasma power. Figure 5(b) shows the pictures of SOPs taken when increasing the gap distance. For the extreme gap distance (i.e., 1 and 10 mm), SOPs show diameters lower than 2mm with a poor discretization level. At intermediate gap distances such as 5–6 mm, SOP diameters become closer to 4mm and present a higher level of discretization.

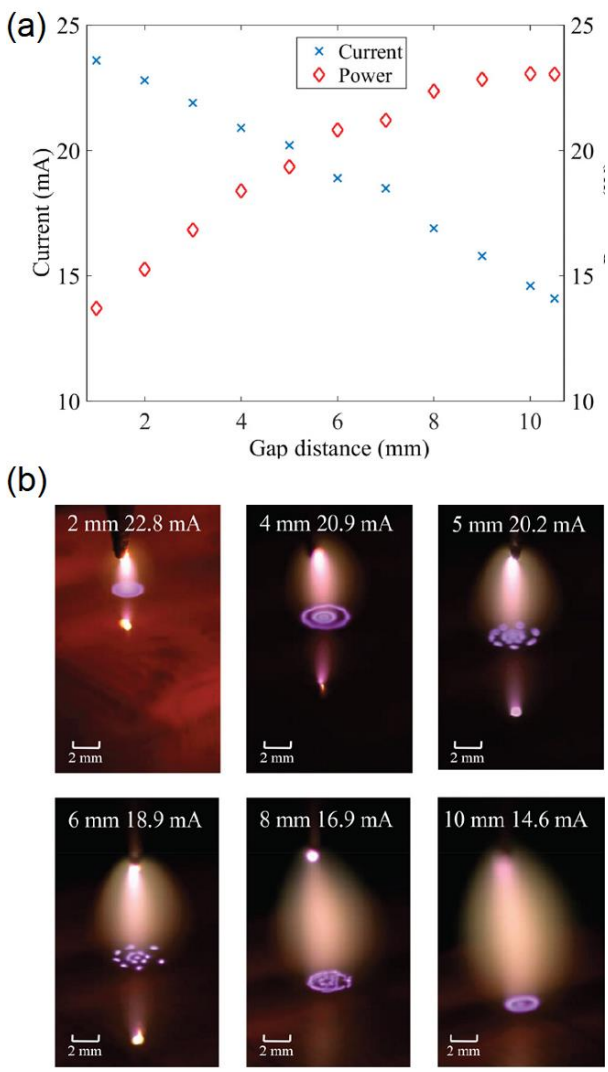

Fig. 5. (a) Current and power dependence on the gap distance and (b) the corresponding formed SOP. The overall discharge voltage is 3200 V. Tap water is employed, and the electric conductivity is 3.08 mS/cm. The exposure time of the images in (b) is 8 ms, and the gap distance is also marked on each image.

III.C.2. Discussion on the SOPs' evolution with the gap distance

To sustain the DC discharge at larger gap, a higher discharge voltage would be necessary. However, the average electric field in the plasma bulk would simultaneously decrease, hence leading to a plausible decrease in the discharge current according to (1):

$$j = e.n_e.\mu_e.E \qquad (1)$$

Changing the gap distance can simultaneously influence the two features of SOPs: SOP diameter and electron density. Their correlation can be studied by crudely estimating the electron density based on Eq. (1) with the following assumptions:

(i) The current density is determined considering the current values reported in Fig. 5(a) and the area of the SOP at the liquid interface.

(ii) Electric field intensity can reasonably be considered as equivalent to that in the plasma bulk since the local increase in the electric field close to the liquid anode takes place within 0.1mm (see above[46])

(iii) The electron mobility is referred to Ref. 49.

(iv) It should be noted that the obtained electron density is equivalent as it cannot discern the negative particle from the electron itself, and here, it is noted as $\bar{n}_e$.

Fig. 6 reports a clear correlation between SOP diameters, $\bar{n}_e$ estimations, and different gap distances. Larger SOP diameters are obtained for intermediate gap distances (3 to 7mm) and for minimum $\bar{n}_e$, around 10^{17} m^{-3}. The smallest diameters of SOPs are obtained at the extreme gap distance (1 and 10.5 mm) and the highest $\bar{n}_e$ value, ≈3×10^{17} m^{-3}. This correlation could also be validated by the results in Sec. III B (not shown in the work).

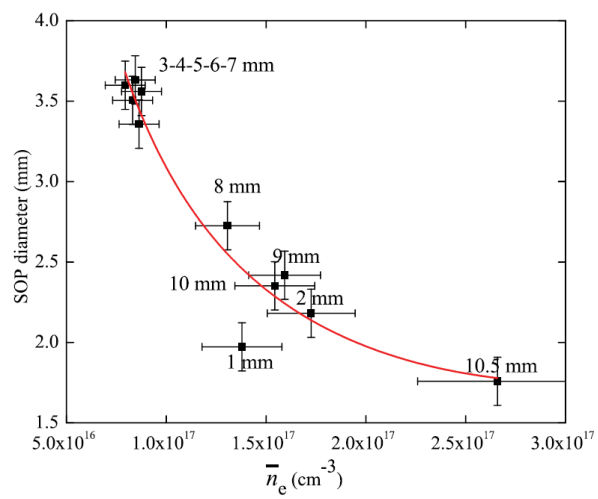

Fig. 6. SOP diameter vs estimated electron density for several gap distances. The gap distance is marked for each data point. The fitting curve is s=1/(0.2464.log($\bar{n}_e$)– 9.322) with 95% confidence bounds.

III.D. Effect of the liquid type on SOP

To verify the SOP dependence on liquid types, a series of experiments are performed where the discharge and setup parameters are identical (same current, same gap distance, and same pin electrode) except the three liquids investigated: sulfuric acid, hydrochloric acid, and hydrofluoric acid. Their pH and EC are listed in Table III.

EC (mS/cm)	pH values	
	H_2SO_4 solution	HCl solution
10	1.56	1.57
57	0.93	0.89
150	0.40	0.33

Table III. EC and the corresponding pH of two types of liquids. Experiments on the other electrolyte solutions have also been performed using NaCl, NaOH, $(NH_4)_2SO_4$ and H_2SO_4 solutions although their effects on SOPs show no unambiguous difference under the same electrical conductivity

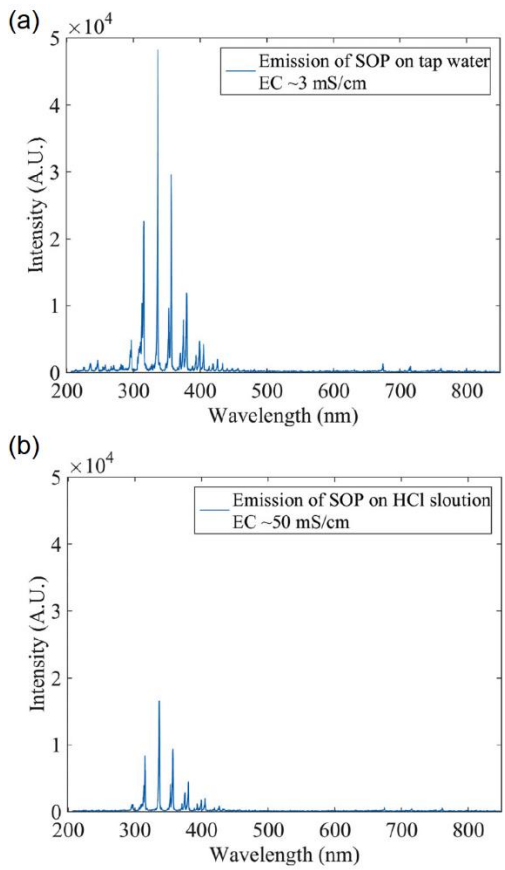

Fig. 7. Emission spectra of SOP from (a) tap water and (b) HCl solution. The exposure time is 50 ms. Note that the emission spectra of SOP from H_2SO_4 solution are also the same as those from HCl solution with only minor different intensity.

III.D.1. SOPs emission spectra under different liquid types

As shown in Fig. 7, changing the liquid type (HCl with 50 mS/cm and tap water with 3 mS/cm, H_2SO_4 solution) does not have influence on the emission spectra of SOPs: the same bands and lines are observed although with different intensities.

III.D.2. SOP characterization with discharge current under H_2SO_4 and HCl solutions

The V–I curves using two acidic solutions at 57 mS/cm and pH (≈0.9) are shown in Fig. 8(a). The two curves overlap and show a decrease in the voltage with the current. Meanwhile, the corresponding SOP formation is shown in Figs. 8(b) and 8(c). Clearly, even with similar electrical properties of the bulk discharge and the EC, the pH values of the anode liquid and the SOPs formed on the H_2SO_4 and HCl interface are significantly different. On one hand, the former remains like those obtained with water: as the current increases, SOPs become more discrete. On the other hand, the SOPs formed on the HCl interface show always a roundish and uniformly emissive pattern.

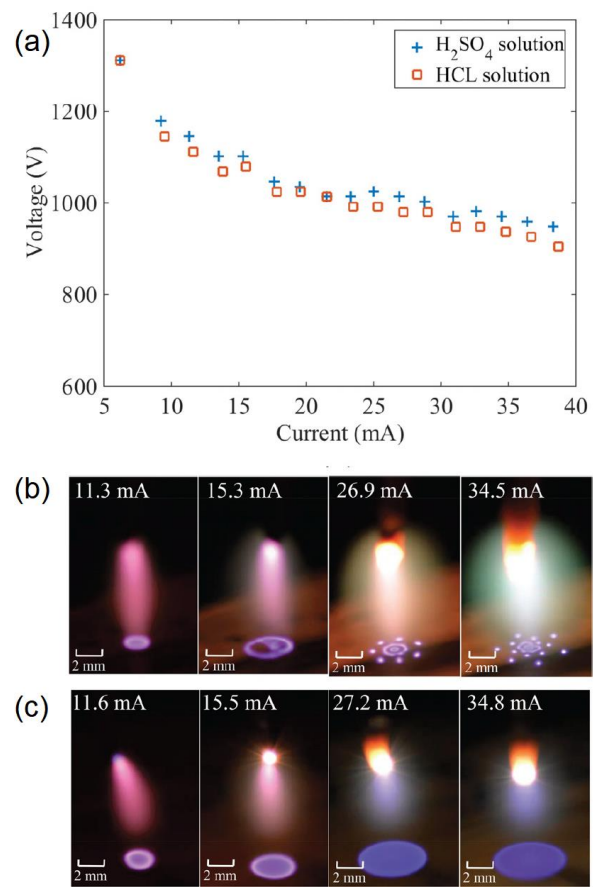

Fig. 8. (a) V-I curve and pictures of SOPs generated on (b) H_2SO_4 and (c) HCl liquid surfaces, gap distance = 5mm, EC(H_2SO_4) = EC(HCl) = 57 mS/cm, and pH(H_2SO_4) = pH(HCl) ≈ 0.9

III.D.3. SOP characterization with the gap distance under H_2SO_4 and HCl solutions

The effect of the gap distance on the discharge current and on SOPs is shown in Fig. 9, always considering H_2SO_4 and HCl solutions at the same electrical conductivity: 57 mS/cm. In Fig. 9(a), an overlap between the two curves is obtained between 1 and 12 mm. Consistent with Figs. 8(b) and 8(c), the SOP shows a discretization feature with H_2SO_4, while it appears as an apparent unique and large spot with HCl. Moreover, SOP diameters reach a maximum value for the intermediate gap distance for both liquids, i.e., 5–6 mm.

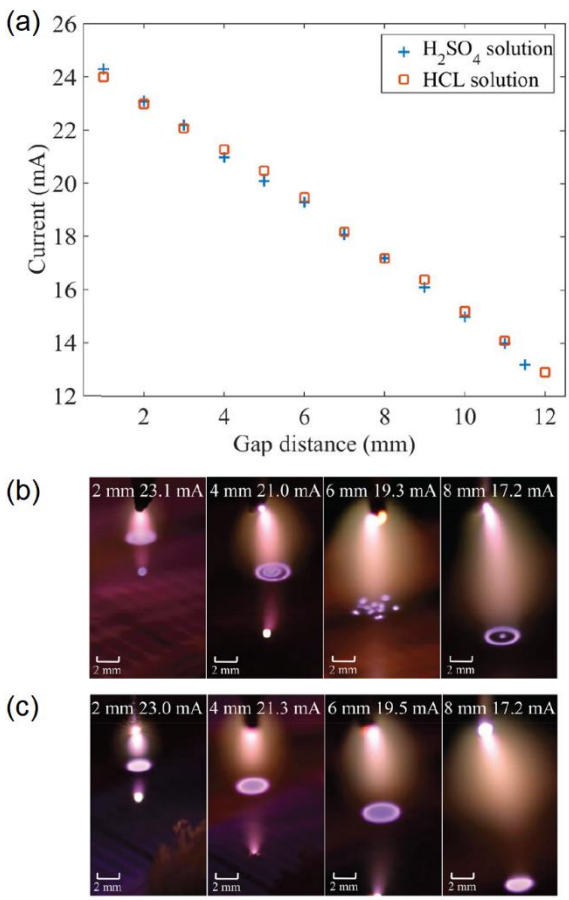

Fig. 9. The dependence of (a) discharge current and SOPs generated with (b) H_2SO_4 and (c) HCl solutions on the gap distance. The discharge voltage is 3200 V, EC(H_2SO_4) = EC(HCl) = 57 mS/cm, and pH(H_2SO_4) = pH(HCl) ≈ 0.9.

III.D.4. SOP characterization with H_2SO_4, HCl, and HF solutions

Figure 10 reports the formation of SOPs on H_2SO_4, HCl, and HF liquid interfaces at the same current (18.7mA 60.6 mA) and gap distances (6.3mm±1.0 mm) but for three electrical conductivities as follows:10, 57, and 150 mS/cm. The electrical conductivity of HF is not acquired with the HANNA conductivity probe to avoid its corrosion. It is estimated based on the HF concentration.[73]

The SOP difference between Figs. 8(b) and 8(c) and Figs. 9(b) and 9(c) still holds for greater EC such as 150 mS/cm with H_2SO_4 and HCl solutions. However, when the electric conductivity is lowered to 10 mS/cm, the SOP of HCl liquid shows a discretization feature as the same as the SOPs of H_2SO_4 solution as shown in Fig. 10(b). The additional SOP formation in Fig. 10(c) with HF solution on the other hand is more like SOP formation with HCl solution when the liquid conductivity increases from 10 mS/cm to 150 mS/cm.

III.D.5. Discussions on the SOP dependence on the liquid type

SOP patterns formed on a liquid surface can be characterized in terms of pattern diameter and discretization. According to SOP appearances in Figs. 8 and 9, the discharge current and gap distance can affect the SOP diameters greatly. The SOP size increases as the discharge current increases with a fixed gap distance. Moreover, the SOP size reaches the maximum at an intermediate gap distance. On the other hand, it is the SOP discretization that significantly depends on the liquid type. Meanwhile, the discretization feature determines the various types of SOPs, such as strips, rings, or spots.

As stated in the works of Shirai et al., replacing the ambient air by nitrogen makes the patterns (see Fig. 13 in Ref. 34) become similar to the ones we obtained when using HCl, as shown in Fig. 8(c). The explanation to their experiment relies on the attachment of free electrons. Since the gas contains no oxygen, the electron attachment strongly decreases to the benefit of higher density of free electrons, which can impinge on the liquid. Moreover, the discharge transits to a column shape if air is replaced by N_2. As a result, this discreet SOP is expected to be obtained only with smaller exposure time, not with 1/30 s in Ref. 34. In the case of the HCl liquid anode, the formed pattern is different from the H_2SO_4 liquid anode but with almost the same discharge current, shape, and gas environment. The underlying mechanism should be different.

Whatever the solution, one can clearly observe in Fig. 10 that (i) for EC as low as 10 mS/cm, the dark region appears narrow, while the SOP exhibits a discreet feature; (ii) for the two larger EC values, a thicker dark region is obtained, while the SOP shows a unique and large spot for HCl and HF solution but not for H_2SO_4; and (iii) whatever the EC or the acid considered, gas bubbles are generated from the immerged anode, evidencing potential electrolysis and therefore the decomposition of the liquid into reactive gaseous species, as reported in Table IV for water, H_2SO_4, HCl, and HF solutions.

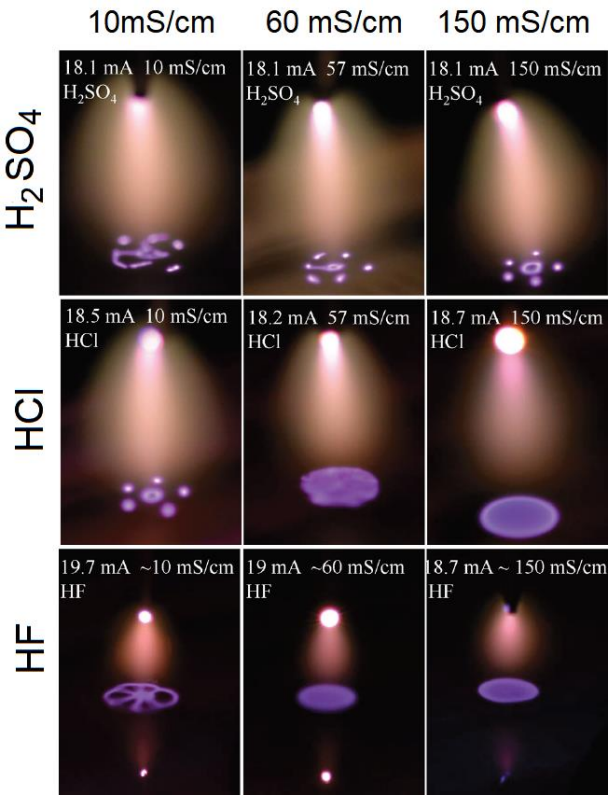

Fig. 10. SOP dependence on the electric conductivity of (a) H2SO4, (b) HCl, and (c) HF electrolyte solutions. The gap distance for H_2SO_4 and HCl solutions is 7 mm, and the overall discharge is 3200 V. The gap distance for HF solution is 5 mm, and the discharge is 3200 V.

As reported in Table IV, for tap water (low EC) and H_2SO_4 solution [high or low EC, also refer to Figs. 8(b) or 9(b)], OH^- is expected to transfer electrons to the anode. For HCl and HF solution (high EC), Cl^- and F^- anions rather than OH^- are oxidized (Table IV). With the highly concentrated HCl or HF electrolyte, gaseous Cl_2 and F_2 are generated and a low but non-negligible portion of the gases crosses the liquid interface into the ambient gas, which corresponds locally to the anode region of the DC discharge and the surrounding ambient air. Henri's law supports the fact that the thermodynamic disequilibrium at the interface is stronger in the case of Cl_2 and F_2 gases since ambient air does not contain any chlorine or fluorine species. The amounts of Cl_2 and F_2 diffused from liquid to gas may hence be slightly higher than O_2.[74]

Electrolyte	Reactions on the anode
Tap water or H_2SO_4 solution	$4OH^-_{(liq)} \rightarrow 2H_2O_{(liq)} + O_{2(g)} + 4e^-$
HCl solution	$2Cl^-_{(liq)} \rightarrow Cl_{2\ \ (g)} + 2e^-$

Table IV. Reactions on the anode in different electrolytes

Once these gases are released, they partly interact with the anode region of the discharge where the electron density is roughly estimated to 10^{17} cm^{-3} (see Fig. 6). In this region, the electrons can interplay with the released electronegative gas, hence leading to the formation of negative ions. The electron affinities of F_2, Cl_2, and O_2 are 3.08 eV, 2.4 eV, and 0.45 eV, respectively.[75] Because F_2 and Cl_2 have higher electron affinities than O_2, one may consider that they penetrate further into the discharge than O_2. Larger electron affinities allow them to interact within the discharge on larger scales, not only on the anode region but also in the dark region, where they could make it thicker compared with tap water or even H_2SO_4 solution.

These negative ions resulting from electron affinity would move back to the liquid anode surface. The impact by these negative ions, which is also highly reactive with water itself, leads finally to different reaction on the water surface. Because SOPs are assumed to be a reaction-diffusion system,[43] different reactions would change SOPs. In a word, the electrolysis process in Table IV may lead to the different patterns of HCl and HF solutions.

As to the dependence on electric conductivity of the SOP, the local electric field at the interface might increase with the electrolyte concentration (electric conductivity here).[76] The increased electric field finally alters the behavior of the SOPs when EC of solution changes.

It should be noted that Table IV is obtained under the frame of conventional electrolysis. However, it should be kept in mind that the electro-chemical reactions of plasma in contact with liquid are different from those of the conventional electrolysis. For example, the electron temperature in this work is around 1 or 2 orders of magnitude higher than that of conventional electrolysis.[2] This high energy may result in efficient reaction $2H^+ + 2e^- \rightarrow H_2(g)$,[77] which should be the reason why there is no H_α or H_β line observed at the interface of plasma and liquid in Sec. IIIA. Moreover, after electrons with several eV energy are solved into the interface, the hydrated electrons can involve more than one chemical reaction[2,78] and might lead to different gas production processes. Additionally, charge transfer via electronegative ions is also possible for plasma in contact with liquid. More difference could be referred to Refs. 2, 78, and 79.

IV. Conclusions

The formation of SOPs in a DC pin liquid anode discharge in air was investigated. The discharge characteristics and the dependence of SOPs on discharge currents and the gap distance with the tap water anode were presented. A stratified discharge is formed in air with a dark region formed above luminous SOPs. Based on the emission spectra of the SOPs, it is the transition of $N_2(C^3\Pi\text{-}B^3\Pi)$ that forms the SOP emission. Meanwhile, $N_2(C)$ is excited in air by energetic electrons, which should be heated due to the local increase in the electric field at the interface.

The size of the SOPs would increase with the discharge current when the gap distance is fixed. If the gap distance increases, the size has the maximum area at the intermediate gap distance. The size evolution of SOPs quite reciprocally correlates with the local electron density as is simulated.

The SOPs behave discrete (more isolate spots) when the discharge current increases at a certain gap distance. However, when the gap distance changes, the SOPs have a higher discrete degree at an intermediate distance.

However, this discrete feature has a liquid type dependence. For HCl and HF solutions with an electric conductivity larger than 57 mS/cm, the SOPs hold a whole round area (large and single spot) with almost no visible discreteness. For H_2SO_4 solution, SOPs behave as tap water no matter how large the electric conductivity is. The relationship between the SOPs and electrolysis is initially discussed. This discovery may shed light on the correlation between the formation mechanisms of SOPs and the electrolysis process in the solution.

V. Acknowledgments

This work was carried out within the LABEX Plas@Par project and received financial state aid managed by the Agence Nationale de la Recherche, as part of the Programme Investissements d'Avenir (PIA) under the Reference No. ANR-11-IDEX-0004-02. The authors thank F. Leblanc for providing the DC power supply. S. Z. thanks Professor Peter Bruggeman for the scientific advice. The authors also greatly thank the referees for their valuable comments.

VI. References

[1]B. R. Locke and K.-Y. Shih, "Review of the methods to form hydrogen peroxide in electrical discharge plasma with liquid water," Plasma Sources Sci. Technol. 20, 034006 (2011).

[2]P. Bruggeman, M. J. Kushner, B. R. Locke, J. Gardeniers, W. Graham, D. B. Graves, R. Hofman-Caris, D. Maric, J. P. Reid, E. Ceriani et al., "Plasma–liquid interactions: A review and roadmap," Plasma Sources Sci. Technol. 25, 053002 (2016).

[3]B. Surowsky, O. Schl€uter, and D. Knorr, "Interactions of non-thermal atmospheric pressure plasma with solid and liquid food systems: A review," Food Eng. Rev. 7, 82–108 (2015).

[4]S. Zhang, A. Rousseau, and T. Dufour, "Promoting lentil germination and stem growth by plasma activated tap water, demineralized water and liquid fertlizer," RSC Adv. 7, 31244–31251 (2017).

[5]Q. Chen, J. Li, and Y. Li, "A review of plasma–liquid interactions for nanomaterial synthesis," J. Phys. D: Appl. Phys. 48, 424005 (2015).

[6]P. Rumbach and D. Go, "Perspectives on plasmas in contact with liquids for chemical processing and materials synthesis," Top. Catal. 60, 799 (2017).

[7]J. E. Foster, "Plasma-based water purification: Challenges and prospects for the future," Phys. Plasmas 24, 055501 (2017).

[8]Y. Gorbanev, D. O'Connell, and V. Chechik, "Non-thermal plasma in contact with water: The origin of species," Chem. Eur. J. 22, 3496–3505 (2016).

[9]N. Kurake, H. Tanaka, K. Ishikawa, K. Takeda, H. Hashizume, K. Nakamura, H. Kajiyama, T. Kondo, F. Kikkawa, M. Mizuno et al., "Effects of OH and NO radicals in the aqueous phase on H2O2 and generated in plasma-activated medium," J. Phys. D: Appl. Phys. 50, 155202 (2017).

[10]Q.-Y. Nie, C.-S. Ren, D.-Z. Wang, S.-Z. Li, J.-L. Zhang, and M. G. Kong, "Self-organized pattern formation of an atmospheric pressure plasma jet in a dielectric barrier discharge configuration," Appl. Phys. Lett. 90, 221504 (2007).

[11]H. Itoh and S. Suzuki, "Hexagonal arrayed patterns with bright and dark spots observed in a compact plasma reactor based on a piezoelectric transformer," Plasma Sources Sci. Technol. 23, 054014 (2014).

[12]H. Purwins and L. Stollenwerk, "Synergetic aspects of gas discharge: Lateral patterns in dc systems with a high ohmic barrier," Plasma Phys. Controlled Fusion 56, 123001 (2014).

[13]E. Gurevich, A. Zanin, A. Moskalenko, and H.-G. Purwins, "Concentricring patterns in a dielectric barrier discharge system," Phys. Rev. Lett. 91, 154501 (2003).

[14]S. Stauss, H. Muneoka, N. Ebato, F. Oshima, D. Pai, and K. Terashima, "Self-organized pattern formation in helium dielectric barrier discharge cryoplasmas," Plasma Sources Sci. Technol. 22, 025021 (2013).

[15]Y. P. Raizer and M. Mokrov, "Physical mechanisms of self organization and formation of current patterns in gas discharges of the townsend and glow types," Phys. Plasmas 20, 101604 (2013).

[16]W. Liu, L. Dong, Y. Wang, H. Zhang, and Y. Pan, "Pattern formation based on complex coupling mechanism in dielectric barrier discharge," Phys. Plasmas 23, 082307 (2016).

[17]Z. Liu, D. Liu, D. Xu, H. Cai, W. Xia, B. Wang, Q. Li, and M. G. Kong, "Two modes of interfacial pattern formation by atmospheric pressure helium plasma jet-ito interactions under positive and negative polarity," J. Phys. D: Appl. Phys. 50, 195203 (2017).

[18]Ruma, S. Hosseini, K. Yoshihara, M. Akiyama, T. Sakugawa, P. Lukes, and H. Akiyama, "Properties of water surface discharge at different pulse repetition rates," J. Appl. Phys. 116, 123304 (2014).

[19]P. Zheng, X. Wang, J. Wang, B. Yu, H. Liu, B. Zhang, and R. Yang, "Self-organized pattern formation of an atmospheric-pressure, ac glow discharge with an electrolyte electrode," Plasma Sources Sci. Technol. 24, 015010 (2014).

[20]K. H. Schoenbach, M. Moselhy, and W. Shi, "Self-organization in cathode boundary layer microdischarges," Plasma Sources Sci. Technol. 13, 177 (2004).

[21]M. Benilov, "Comment on 'self-organization in cathode boundary layer discharges in xenon' and 'self-organization in cathode boundary layer microdischarges'," Plasma Sources Sci. Technol. 16, 422 (2007).

[22]W. Zhu and P. Niraula, "The missing modes of self-organization in cathode boundary layer discharge in xenon," Plasma Sources Sci. Technol. 23, 054011 (2014).

[23]W. Zhu, P. Niraula, P. Almeida, M. Benilov, and D. Santos, "Self-organization in dc glow microdischarges in krypton: Modelling and experiments," Plasma Sources Sci. Technol. 23, 054012 (2014).

[24]N. Takano and K. H. Schoenbach, "Self-organization in cathode boundary layer discharges in xenon," Plasma Sources Sci. Technol. 15, S109 (2006).

[25]Y. A. Astrov, A. Lodygin, and L. Portsel, "Self-organized patterns in successive bifurcations in planar semiconductor-gas-discharge device," Phys. Rev. E 91, 032909 (2015).

[26]C. Maszl, J. Laimer, and H. Stori, "Observations of self-organized luminous patterns on the anode of a direct-current glow discharge at higher pressures," IEEE Trans. Plasma Sci. 39, 2118–2119 (2011).
[27]V. Arkhipenko, T. Callegari, Y. Safronau, L. Simonchik, and I. Tsuprik, "Anode spot patterns and fluctuations in an atmospheric-pressure glow discharge in helium," Plasma Sources Sci. Technol. 22, 045003 (2013).
[28]G. Mackay, "Symmetrical subdivision of anode glow in helium discharge tubes," Phys. Rev. 15, 309 (1920).
[29]C. H. Thomas and O. Duffendack, "Anode spots and their relations to the absorption and emission of gases by the electrodes of a Geissler discharge," Phys. Rev. 35, 72 (1930).
[30]S. M. Rubens and J. Henderson, "The characteristics and function of anode spots in glow discharges," Phys. Rev. 58, 446 (1940).
[31]K. Emeleus, "Anode glows in glow discharges: Outstanding problems," Int. J. Electron. Theor. Exp. 52, 407–417 (1982).
[32]K. Meuller, "Structures at the electrodes of gas discharges," Phys. Rev. A 37, 4836 (1988).
[33]N. Shirai, S. Uchida, F. Tochikubo, and S. Ishii, "Self-organized anode pattern on surface of liquid or metal anode in atmospheric dc glow discharges," IEEE Trans. Plasma Sci. 39, 2652–2653 (2011).
[34]N. Shirai, S. Uchida, and F. Tochikubo, "Influence of oxygen gas on characteristics of self-organized luminous pattern formation observed in an atmospheric dc glow discharge using a liquid electrode," Plasma Sources Sci. Technol. 23, 054010 (2014).
[35]S. Xu and X. Zhong, "Self-deformation in a direct current driven helium jet micro discharge," Phys. Plasmas 23, 010701 (2016).
[36]A. Wilson, D. Staack, T. Farouk, A. Gutsol, A. Fridman, and B. Farouk, "Self-rotating dc atmospheric-pressure discharge over a water-surface electrode: Regimes of operation," Plasma Sources Sci. Technol. 17, 045001 (2008).
[37]T. Verreycken, P. Bruggeman, and C. Leys, "Anode pattern formation in atmospheric pressure air glow discharges with water anode," J. Appl. Phys. 105, 083312 (2009).
[38]Z. Chen, S. Zhang, I. Levchenko, I. I. Beilis, and M. Keidar, "In vitro demonstration of cancer inhibiting properties from stratified self-organized micro-discharge plasma-liquid interface," Sci. Rep. 7, 12163 (2017).
[39]T. Callegari, B. Bernecker, and J. Boeuf, "Pattern formation and dynamics of plasma filaments in dielectric barrier discharges," Plasma Sources Sci. Technol. 23, 054003 (2014).
[40]N. Y. Babaeva and M. J. Kushner, "Self-organization of single filaments and diffusive plasmas during a single pulse in dielectric-barrier discharges," Plasma Sources Sci. Technol. 23, 065047 (2014).
[41]J. P. Trelles, "Electrode patterns in arc discharge simulations: Effect of anode cooling," Plasma Sources Sci. Technol. 23, 054002 (2014).
[42]J. P. Trelles, "Pattern formation and self-organization in plasmas interacting with surfaces," J. Phys. D: Appl. Phys. 49, 393002 (2016).
[43]M. Benilov, "Multiple solutions in the theory of dc glow discharges and cathodic part of arc discharges. application of these solutions to the modeling of cathode spots and patterns: A review," Plasma Sources Sci. Technol. 23, 054019 (2014).
[44]M. Bieniek, P. G. Almeida, and M. S. Benilov, "Self-consistent modelling of self-organized patterns of spots on anodes of dc glow discharges," Plasma Sources Sci. Technol. 27, 05LT03 (2018).
[45]J. P. Trelles, "Formation of self-organized anode patterns in arc discharge simulations," Plasma Sources Sci. Technol. 22, 025017 (2013).
[46]R. Gopalakrishnan, E. Kawamura, A. Lichtenberg, M. Lieberman, and D. Graves, "Solvated electrons at the atmospheric pressure plasma–water anodic interface," J. Phys. D: Appl. Phys. 49, 295205 (2016).
[47]J. Winter, K. Wende, K. Masur, S. Iseni, M. Dünnbier, M. Hammer, H. Tresp, K. Weltmann, and S. Reuter, "Feed gas humidity: A vital parameter affecting a cold atmospheric-pressure plasma jet and plasma-treated human skin cells," J. Phys. D: Appl. Phys. 46, 295401 (2013).
[48]Q. Xiong, Z. Yang, and P. J. Bruggeman, "Absolute oh density measurements in an atmospheric pressure dc glow discharge in air with water electrode by broadband uv absorption spectroscopy," J. Phys. D: Appl. Phys. 48, 424008 (2015).
[49]Y. P. Raizer and J. E. Allen, Gas Discharge Physics (Springer, Berlin, 1997), Vol. 2.
[50]P. Bruggeman, J. Liu, J. Degroote, M. G. Kong, J. Vierendeels, and C. Leys, "Dc excited glow discharges in atmospheric pressure air in pin-to-water electrode systems," J. Phys. D: Appl. Phys. 41, 215201 (2008).
[51]J. Park, P. Kostyuk, S. Han, J. Kim, C. Vu, and H. Lee, "Study on optical emission analysis of ac air–water discharges under He, Ar and N_2 environments," J. Phys. D: Appl. Phys. 39, 3805 (2006).
[52]P. Hoffer, Y. Sugiyama, S. H. R. Hosseini, H. Akiyama, P. Lukes, and M. Akiyama, "Characteristics of meter-scale surface electrical discharge propagating along water surface at atmospheric pressure," J. Phys. D: Appl. Phys. 49, 415202 (2016).
[53]V. V. Kovacˇevic´, B. P. Dojcˇinovic´, M. Jovic´, G. M. Roglic´, B. M. Obradovic´, and M. M. Kuraica, "Measurement of reactive species generated by dielectric barrier discharge in direct contact with water in different atmospheres," J. Phys. D: Appl. Phys. 50, 155205 (2017).
[54]P. Lu, D. Boehm, P. Bourke, and P. J. Cullen, "Achieving reactive species specificity within plasma-activated water through selective generation using air spark and glow discharges," Plasma Processes Polymers 14, e1600207 (2017).
[55]Y. Itikawa and N. Mason, "Cross sections for electron collisions with water molecules," J. Phys. Chem. Ref. data 34, 1–22 (2005).
[56]P. Bruggeman, N. Sadeghi, D. Schram, and V. Linss, "Gas temperature determination from rotational lines in non-equilibrium plasmas: A review," Plasma Sources Sci. Technol. 23, 023001 (2014).
[57]R. Riahi, P. Teulet, Z. B. Lakhdar, and A. Gleizes, "Cross section and rate coefficient calculation for electron impact excitation, ionisation and dissociation of H2 and OH molecules," Eur. Phys. J. D 40, 223–230 (2006).
[58]T. Millar, P. Farquhar, and K. Willacy, "The UMIST database for astrochemistry 1995," Astron. Astrophys. Suppl. Ser. 121, 139–185 (1997).
[59]I. Kossyi, A. Y. Kostinsky, A. Matveyev, and V. Silakov, "Kinetic scheme of the non-equilibrium discharge in nitrogen-oxygen mixtures," Plasma Sources Sci. Technol. 1, 207 (1992).
[60]J. Bacri and A. Medani, "Electron diatomic molecule weighted total cross section calculation: III. Main inelastic processes for n2 and n+2," Physica B 112, 101–118 (1982).
[61]L. G. Piper, "State-to-state N2 (a3σ+u) energy-pooling reactions. I. The formation of n2 (c3πu) and the Herman infrared system," J. Chem. Phys. 88, 231–239 (1988).
[62]J. T. Herron and D. S. Green, "Chemical kinetics database and predictive schemes for nonthermal humid air plasma chemistry. Part II. Neutral species reactions," Plasma Chem. Plasma Process. 21, 459–481 (2001).
[63]T. Verreycken, "Spectroscopic investigation of OH dynamics in transient atmospheric pressure plasmas," Ph.D. thesis (Technische Universiteit Eindhoven, Eindhoven, The Netherlands, 2013).

[64]V. Arkhipenko, A. Kirillov, Y. A. Safronau, L. Simonchik, and S. Zgirouski, "Self-sustained dc atmospheric pressure normal glow discharge in helium: From microamps to amps," Plasma Sources Sci. Technol. 18, 045013 (2009).
[65]S. Kanazawa, H. Kawano, S. Watanabe, T. Furuki, S. Akamine, R. Ichiki, T. Ohkubo, M. Kocik, and J. Mizeraczyk, "Observation of OH radicals produced by pulsed discharges on the surface of a liquid," Plasma Sources Sci. Technol. 20, 034010 (2011).
[66]S. Zhang, W. van Gaens, B. van Gessel, S. Hofmann, E. van Veldhuizen, A. Bogaerts, and P. Bruggeman, "Spatially resolved ozone densities and gas temperatures in a time modulated rf driven atmospheric pressure plasma jet: An analysis of the production and destruction mechanisms," J. Phys. D: Appl. Phys. 46, 205202 (2013).
[67]A. van Gessel, K. Alards, and P. Bruggeman, "No production in an rf plasma jet at atmospheric pressure," J. Phys. D: Appl. Phys. 46, 265202 (2013).
[68]M. Simek, S. DeBenedictis, G. Dilecce, V. Babicky` , M. Clupek, and P. Sunka, "Time and space resolved analysis of N2 (c3πu) vibrational distributions in pulsed positive corona discharge," J. Phys. D: Appl. Phys. 35, 1981 (2002).
[69]M. Laroussi, X. Lu, and C. M. Malott, "A non-equilibrium diffuse discharge in atmospheric pressure air," Plasma Sources Sci. Technol. 12, 53 (2003).
[70]S. Chen and R. J. Anderson, "Excitation of the c 3πu state of N_2 by electron impact," J. Chem. Phys. 63, 1250–1254 (1975).
[71]O. Dutuit, A. Tabche-Fouhaile, I. Nenner, H. Frohlich, and P. Guyon, "Photodissociation processes of water vapor below and above the ionization potential," J. Chem. Phys. 83, 584–596 (1985).
[72]M. A. Lieberman and A. J. Lichtenberg, Principles of Plasma Discharges and Materials Processing (John Wiley & Sons, 2005).
[73]S. Broderick, "Conductivity of hydrofluoric acid solutions and the effect of the impurities, sulfurous and hydrofluosilicic acids," J. Chem. Eng. Data 7, 55–57 (1962).
[74]R. Sander, "Compilation of Henry's law constants (version 4.0) for water as solvent," Atmos. Chem. Phys. 15, 4399–4981 (2015).
[75]M. T. Bowers, Gas Phase Ion Chemistry (Academic Press, 1979), Vol. 2.
[76]P. Rumbach, J. P. Clarke, and D. B. Go, "Electrostatic Debye layer formed at a plasma-liquid interface," Phys. Rev. E 95, 053203 (2017).
[77]M. Witzke, P. Rumbach, D. B. Go, and R. M. Sankaran, "Evidence for the electrolysis of water by atmospheric-pressure plasmas formed at the surface of aqueous solutions," J. Phys. D: Appl. Phys. 45, 442001 (2012).
[78]F. Tochikubo, Y. Shimokawa, N. Shirai, and S. Uchida, "Chemical reactions in liquid induced by atmospheric-pressure dc glow discharge in contact with liquid," Jpn. J. Appl. Phys., Part 1 53, 126201 (2014).
[79]S. K. S. Gupta, "Contact glow discharge electrolysis: Its origin, plasma diagnostics and non-faradaic chemical effects," Plasma Sources Sci. Technol. 24, 063001 (2015).